United States Department of Commerce
Technology Administration
National Institute of Standards and Technology

NIST Technical Note 1388

Toward Extended-Cavity Grating-Tuned Mid-Infrared Diode Laser Operation

Manfred Mürtz
Joseph S. Wells
Leo Hollberg
Tamara Zibrova
Neil Mackie

NIST Technical Note 1388

Toward Extended-Cavity Grating-Tuned Mid-Infrared Diode Laser Operation

Manfred Mürtz
Joseph S. Wells
Leo Hollberg
Tamara Zibrova
Neil Mackie

Time and Frequency Division
Physics Laboratory
National Institute of Standards and Technology
325 Broadway
Boulder, Colorado 80303-3328

August 1997

U.S. DEPARTMENT OF COMMERCE, William M. Daley, Secretary
TECHNOLOGY ADMINISTRATION, Gary R. Bachula, Acting Under Secretary for Technology
NATIONAL INSTITUTE OF STANDARDS AND TECHNOLOGY, Robert E. Hebner, Acting Director

National Institute of Standards and Technology Technical Note
Natl. Inst. Stand. Technol., Tech. Note 1388, 28 pages (August 1997)
CODEN:NTNOEF

U.S. GOVERNMENT PRINTING OFFICE
WASHINGTON: 1997

For sale by the Superintendent of Documents, U.S. Government Printing Office, Washington, DC 20402-9325

Contents

Toward Extended-Cavity Grating-Tuned Mid-Infrared Diode Laser Operation

Manfred Mürtz*, Joseph S. Wells, Leo Hollberg,
Tamara Zibrova, and Neil Mackie

Time and Frequency Division
National Institute of Standards and Technology
Boulder, CO 80303, USA

Abstract

We have investigated an extended-cavity technique which utilizes tunable lead-salt diode lasers, emitting in the spectral region around 3 μm. We have developed a special liquid-nitrogen cryostat that enables us to place both the collimation optics and the optics for the extended cavity within the vacuum chamber. The external reflector is a diffraction grating for wavelength-selective optical feedback. This scheme promises to overcome two major drawbacks of tunable diode lasers, their large spectral width and their incomplete spectral coverage. Progress with the coating efforts, problems with the collimation optics, and establishment of procedures for determining optimum feedback are discussed.

Keywords:
cryogenically cooled diode laser, extended-cavity grating-tuned diode laser, InAsSb diode laser, mid-infrared diode laser, optical feedback, tunable diode laser

Permanent address:
Institut für Angewandte Physik der Universität Bonn, D-53115 Bonn, Germany

1 Introduction

Lead-salt tunable diode lasers (TDL) are widely used laser sources in the mid-infrared spectral region between 3 and 30 μm. Advantages compared to other lasers in this spectral region (e.g., molecular gas lasers) are their frequency tunability and compactness. On the other hand, they exhibit several disadvantages such as the cryogenic cooling requirement, the relatively large linewidth, and the fairly complex mode behavior. Moreover, there are gaps in the spectral coverage of a single TDL due to mode jumps. The benefit of lead-salt lasers would be greater if we could overcome these difficulties. The application of TDLs for sub-Doppler molecular spectroscopy or optical frequency synthesis requires a substantial improvement of the spectral properties. A promising approach to reduce the linewidth of diode lasers is the method of external optical feedback. This technique is well-studied and widely used for line narrowing of III-V semiconductor lasers (based on GaAs and InP) which usually emit in the visible and near-infrared.[1] In comparison to these lasers, lead-salt diode-laser research and development is still in the early stages. Typical mid-infrared lasers have a much less sophisticated structure to confine electrons and photons, much higher intrinsic loss, lower internal quantum efficiency, and consequently show multi-mode emission and relatively low output power. Moreover, the work with mid-infrared lasers is complicated because they must sit in a vacuum chamber and the beam is not visually observable. Nevertheless, the investigation of TDLs with weak external optical feedback was initiated at the Institute of Applied Physics at the University of Bonn in 1992 [1]. This work led to an optically stabilized TDL system with a 200 kHz linewidth [2]. A major drawback of this system is the restricted continuous tuning range.

The successful experiments in Bonn gave the impetus to develop a further improved TDL system at NIST, Boulder. It is based on an anti-reflection (AR) coated diode laser, sitting in a vacuum chamber which also contains the optics for the extended cavity, especially the echelette grating for wavelength tuning. In this report we describe this new TDL system and identify some remaining problems.

[1] Very recently the upper wavelength edge of III-V laser operation has been shifted towards 3.5 μm.

2 Extended-Cavity Considerations

Detailed explanations of the operation of diode lasers in extended cavities can be found in References [3, 4, 5, 6] and references therein. Here we intend to introduce some basic concepts and terms and present the principal ideas of the work.

2.1 Extended-Cavity Techniques

Putting a diode laser into an external cavity offers several advantages. First, the enhanced photon lifetime in the cavity leads to narrower spectral width of the external-cavity laser (ECL) emission. Second, a properly designed ECL will operate on a single external-cavity mode. Third, the use of an external wavelength filter allows tunability across the wide-gain bandwidth of the diode laser.

The most common ECLs operate in the strong-external-feedback regime. This requires at least one of the diode laser facets to have a dielectric AR coating. A configuration where only one facet is AR coated is called an *extended-cavity configuration.* The opposite side, which is uncoated (or sometimes coated to be highly reflective), serves as one end mirror of the cavity. This is the configuration investigated here.

Another possibility is to operate the laser in the weak external feedback regime. This is often called an optical locking technique and can sometimes be applied successfully to lasers without any AR coating. However, such systems are much more difficult to handle due to the composite resonator effects, and one has to be very careful to avoid undesirable effects such as bistability and axial-mode instability.

2.2 Design and Requirements

The new NIST TDL system is designed as an extended-cavity grating-tuned (ECGT) diode laser. That is, the cavity is formed by one facet of the diode and an external reflecting diffraction grating as a tunable wavelength filter. One requirement for operation of such a configuration is that the reflection losses of the solitary diode cavity should be much greater than the combined reflection and coupling losses of the external cavity. At a minimum,

the solitary cavity loss should exceed the external-cavity loss by at least 20 dB [6]. This corresponds to $R_{\text{facet}} < 10^{-2} \times R_{\text{ext}}$ where R_{facet} and R_{ext} are the power reflectance of the output facet and the external feedback optics including coupling losses. This means that one has to take care to achieve a minimum residual reflectance of the facet and a maximum coupling of the return beam from the grating into the diode cavity. These two points are the focus of the work reported here.

The index of refraction of lead-salt semiconductors depends on the composition and is not exactly known for the material used in this work. It is assumed to be in the region between $n = 5$ and $n = 6$. The power reflectance of the bare facet is

$$R = \frac{(n-1)^2}{(n+1)^2} , \tag{1}$$

thus yielding values in the range of $R = 44\%$ to $R = 51\%$.

The most critical optical component of the external cavity is the collimator. This collimator must transform the beam waist at the diode facet into another waist at the surface of the grating. The coupling efficiency depends not only on the attenuation of the collimator, but also on the wavefront distortion. A peak-to-peak wavefront distortion of $\lambda/4$ already results in a 2 dB reduction in coupling efficiency [6].

In the next section we give a brief description of the basic lasing characteristics of an extended-cavity laser, such as laser threshold and slope efficiency, with focus on the role of reflectances of facet and external surface. We also introduce some useful relations which will be employed in Sec. 4.

2.3 Operational Characteristics

The output power versus current (P-I) curve of a diode laser is characterized by the threshold current I_{th} and the slope efficiency $\Delta P/\Delta I$ above threshold (Fig. 1). At lasing threshold the round-trip optical gain by stimulated emission equals the total round-trip loss (if we neglect the contribution of spontaneous emission). The gain coefficient per unit length varies nearly linearly with injected carrier density and is simply given by

$$g(I, \nu) = \gamma \left(I - I_{\text{tr}}(\nu) \right) , \tag{2}$$

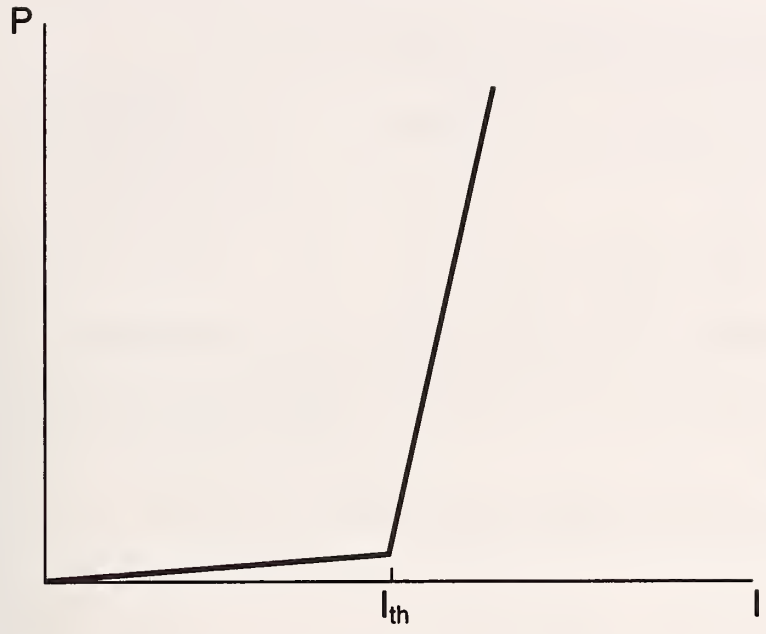

Figure 1: Schematic of light output versus injection current curve (P-I plot) of a diode laser.

where γ is a constant (independent of ν), I is the pump current, and $I_{tr}(\nu)$ is the transparency current. γ is an important constant which characterizes the efficiency of the pump process in the active medium. Major nonradiative (band-to-band) recombination processes which do not contribute to the emission of light are: (a) nonradiative recombination through recombination centers, and (b) recombination due to Auger processes [7]. Auger processes are characterized by the transfer of the excess energy released by the recombination to either an electron or a hole, yielding a hot electron or hot hole. The Auger process becomes more significant as λ increases and its importance in lead-salt devices was pointed out by Emtage [8]. A typical value for γ is 0.4 $\mathrm{mA^{-1}\cdot\ mm^{-1}}$ for a GaAs laser [6]. To our knowledge the value of γ is not known for lead-salt devices.

The round-trip optical loss in the active region is given by a combination of mirror transmission loss and internal photon loss due to free-carrier absorption, scattering, etc. A simple rate equation analysis yields the threshold condition is

$$r_1^2\ r_2^2\ e^{(g_{th}-\alpha_{int})\ 2L_{int}+i\omega\tau_{int}} = 1\ , \tag{3}$$

where r_1, r_2 are the *amplitude* reflectances of the facets, g_{th} is the threshold gain, α_{int} is the internal photon loss, L_{int} is the physical length of the diode cavity, τ_{int} is the internal round-trip time, and ω is the angular frequency of the laser oscillation. The threshold gain

is then determined from the magnitude of the threshold condition (3):

$$g_{\rm th} = \alpha_{\rm int} + \frac{1}{L_{\rm int}} \ln \frac{1}{r_1\, r_2} = \alpha_{\rm int} + \alpha_{\rm mir} \ , \tag{4}$$

where

$$\alpha_{\rm mir} = \frac{1}{L_{\rm int}} \ln \frac{1}{r_1\, r_2} \tag{5}$$

is the mirror transmission loss. Typical values for the mirror loss are on the order of 10^3 m^{-1}. The internal photon loss is typically on the order of 10^3 m^{-1} for GaAs devices, and on the order of 10^5 m^{-1} for lead-salt lasers.

Combining eqs (2) and (4) the threshold current is found to be

$$I_{\rm th} = \frac{1}{\gamma} (\alpha_{\rm int} + \alpha_{\rm mir}) + I_{\rm tr} \ , \tag{6}$$

yielding

$$I_{\rm th} = \frac{1}{\gamma} (\alpha_{\rm int} + \frac{1}{L_{\rm int}} \ln \frac{1}{r_1\, r_2}) + I_{\rm tr} \ . \tag{7}$$

Accordingly, the threshold current of a diode with an AR coating on one side is given by

$$I_{\rm th}^{\rm AR} = \frac{1}{\gamma} (\alpha_{\rm int} + \frac{1}{L_{\rm int}} \ln \frac{1}{r_1\, r_2^*}) + I_{\rm tr} \ , \tag{8}$$

where r_2^* is the residual reflectance of the coated facet.

In the case of an extended-cavity laser, the coupling facet and the external reflector form a compound mirror, resulting in an effective reflectance of the extended cavity given by [9]

$$r_{\rm eff}(\omega) = \frac{r_2^* + r_{\rm ext}\, {\rm e}^{i\omega\tau_{\rm ext}}}{1 + r_2^*\, r_{\rm ext}\, {\rm e}^{i\omega\tau_{\rm ext}}} \ , \tag{9}$$

where $r_{\rm ext}$ is the reflectance of the external reflector. Thus, regarding threshold behavior, the ECL can be considered as a solitary diode laser with a frequency-dependent mirror transmission loss at the coated side. This frequency dependence is a compound-cavity effect; the external reflectance is not assumed to be frequency dependent here. The result is a ripple pattern on the P-I curve. By averaging over this ripple, we obtain the average threshold current of the ECL (according to eq (6)):

$$I_{\rm th}^{\rm ECL} = \frac{1}{\gamma} (\alpha_{\rm int} + \bar{\alpha}_{\rm mir}) + I_{\rm tr} \ , \tag{10}$$

Table 1: Typical laser parameters.

Parameter	Symbol	Lead-salt DL	GaAs DL
threshold current	$I_{\rm th}$	> 100 mA	< 50 mA
ext. quantum efficiency	$\eta_{\rm ext}$	$< 1\%$	50%
refractive index	n	5–6	3–4
cavity length	$L_{\rm int}$	300–600 μm	200–500 μm
cavity round-trip time	$\tau_{\rm int}$	10^{-11} s	10^{-11} s
facet amplitude reflectance	r_1, r_2	60–70%	50–60%
mirror transmission loss	$\alpha_{\rm mir}$	10^3 m^{-1}	10^3 m^{-1}
internal photon loss	$\alpha_{\rm int}$	10^5 m^{-1} †	10^3 m^{-1}
internal gain	γ	unknown	0.4 mA$^{-1}\cdot$ mm^{-1}

† estimated from typical external efficiency, assuming that the internal quantum efficiency is close to 1

yielding

$$I_{\rm th}^{\rm ECL} = \frac{1}{\gamma}(\alpha_{\rm int} + \frac{1}{L_{\rm int}} \ln \frac{1}{r_1\, \bar{r}_{\rm eff}}) + I_{\rm tr} \ , \tag{11}$$

where $\bar{\alpha}_{\rm mirr}$ and $\bar{r}_{\rm eff}$ are the frequency-averaged quantities.

Above threshold, the relation between output power $P_{\rm out}$ (from both facets) and injection current I is given by

$$P_{\rm tot} = \frac{h\nu}{e}\, \eta_{\rm ext}(I - I_{\rm th}) \ . \tag{12}$$

$\eta_{\rm ext}$ is called the differential external quantum efficiency and is given by

$$\eta_{\rm ext} = \eta_{\rm int} \frac{\alpha_{\rm mir}}{\alpha_{\rm mir} + \alpha_{\rm int}} \ , \tag{13}$$

where $\eta_{\rm int}$ is the internal quantum efficiency of the stimulated emission. $\eta_{\rm int}$ gives the probability of radiative recombination for carriers injected into the active region well above threshold. The quantity $\eta_{\rm int}$ is assumed to be close to 1 (due to the carrier density clamping). Typical values of the differential external efficiency of lead-salt lasers are in the range of 0.1% to 1% depending on the laser material and cavity structure. Substituting $\alpha_{\rm mir}$ in eq (13) and combining with eq (5), we obtain the relation

$$\eta_{\rm ext} = \eta_{\rm int}\, (1 + \alpha_{\rm int}\ L_{\rm int} / \ln \frac{1}{r_1\ r_2})^{-1} \tag{14}$$

for the differential external quantum efficiency.

Equation (12) gives only the total optical output power from both laser facets. If one facet is AR coated, the slope efficiency $\Delta P/\Delta I$ changes depending on which side is under observation. The slope efficiencies observed at facet 1 and 2, respectively, are given by [4]

$$\frac{\Delta P_1}{\Delta I} = \frac{h\nu}{e}\,\eta_{\text{ext}} \times \frac{(1-r_1^2)\,r_2}{(r_1+r_2)(1-r_1r_2)} \tag{15}$$

and

$$\frac{\Delta P_2}{\Delta I} = \frac{h\nu}{e}\,\eta_{\text{ext}} \times \frac{(1-r_2^2)\,r_1}{(r_1+r_2)(1-r_1r_2)}\,. \tag{16}$$

Analysis of eqs (15) and (16) shows that, after AR coating, the slope efficiency on the coated side increases, whereas it decreases at the untreated side.

A summary of typical laser parameters of lead-salt diode lasers compared with GaAs type lasers is given in Table 1. A striking difference turns up at the external quantum efficiency and at the internal photon loss parameter.

3 Experimental Details

The experimental arrangement for the extended-cavity lead-salt lasers consists of a vacuum chamber which houses the diode laser as well as the external cavity elements. This set-up and the equipment used to characterize the spectral properties of the lasers are described in this chapter.

3.1 TDL Cryostat

The TDL cryostat chamber is schematically depicted in Fig. 2. It consists of a stainless steel cylinder (outer diameter = 32 cm) which is closed with a glass lid. A cold foot made of oxygen-free high conductivity (OFHC) copper is attached to the OFHC copper portion of the liquid nitrogen tail. This is attached to an OFHC copper bar which is supported by a temperature isolating post attached to the support frame. The frame can be adjusted in two directions; vertical adjustment is made by means of shims below the isolation post. The nitrogen hold time of the cryostat is about 6 h, and the temperature at the laser during

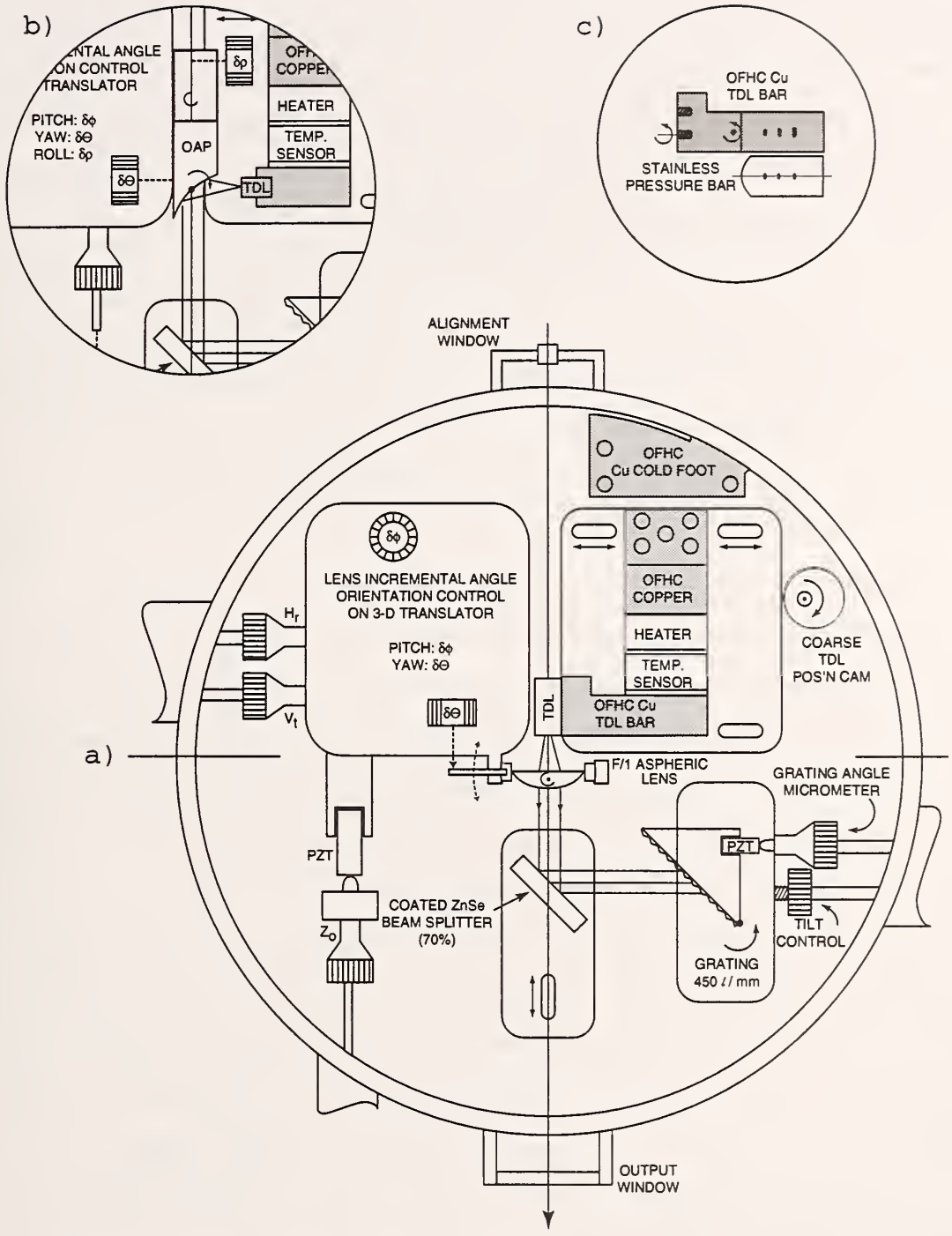

Figure 2: (a) Arrangement of the cryostat chamber for an ECGT-TDL. Inset (b) shows the off-axis parabola which was used for collimation during the initial stage of the work. Inset (c) shows details of the OFHC copper bar for mounting the diode laser.

operation is only a few Kelvin above 77 K. The chamber is evacuated by means of an oil diffusion pump through a cold trap.

During the initial stage of this project, the collimation of the TDL beam was performed by means of an off-axis parabolic mirror (f = 10.2 mm) (inset (b) of Fig. 2). This mirror sits on a high precision three-dimensional (3D) translation stage which can be controlled by retractable rods from outside the chamber. In the course of the experiments, the parabola was replaced with a lens (Sec. 4.2). This required some modifications of the 3D mount as well as at the cold station for the TDL. This design has continued to evolve as dictated by the results of the latest experiments. A new aspheric lens provided better coupling between the laser chip mode and the extended cavity, however, the focus adjustment is very sensitive (about 3×10^{-4} of focal length) and required a three level hyperfine control of the focus point. This control is accomplished by means of an externally operated micrometer and a push rod between the micrometer and the 3D translation stage contact point. The micrometer has a 2 mm travel for the usual control, and a portion of the push rod consists of a PZT with a 16 μm travel for the requisite finer manipulation. This turned out to be adequate, since with the coarse control, one can set the lens holder/TDL bar separation to our previously determined value (the prior experiments were made with a temporary long-range micrometer on the top-mounted stage). The coarse adjustment is provided by a slotted mount on top of the 3D translator which is fixed in place after coarse alignment. This top-mounted stage also permitted tilt and yaw adjustments of the lens as shown in Fig. 2.

The ZnSe beam splitter is coated on one side for a power reflectance of 70% at 45° and AR coated on the opposite side. The grating is a 458 line/mm echelette grating with a reflectance of at least 98% in first-order diffraction. It is arranged in a Littrow mount. The grating angle and tilt can also be controlled from outside the chamber by retractable rods. In addition, the grating angle can be scanned through one FSR by means of a PZT (8 μm range) between the micrometer and grating mount contact point. The purpose of this is to facilitate CO laser/TDL frequency overlap for heterodyne beat experiments (Sec. 3.4).

3.2 Alignment Procedure

An important condition for external-cavity operation is a perfect alignment of laser and external optical elements. This is nontrivial and turned out to be laborious since the infrared beam is low power and not visible. We have developed an alignment procedure for use with the TDL chamber, and modified the chamber where necessary. One of the early modifications involved the capability to make slight angular orientation adjustments on the TDL (see Fig. 2, inset (c)). This was necessary because in many cases, the normal to the laser chip was not parallel to the laser submount proper.

The optical layout of the chamber has been discussed. An extension of the optic axis of the ECDL is defined by two irises external to the chamber, one about 30 cm from the chamber window, the second one about 130 cm further downstream. Alignment was made in two phases, one to control the beam direction and waist; the second to optimize the feedback to the TDL.

The first step in phase one was to send a HeNe laser beam backward through the two external irises and into the chamber. The TDL was positioned to have the chip facet in the center of the visible red beam, and then the TDL was oriented so that the red beam was retro-reflected. This was determined by the position of the chip facet reflection at the second iris. The second step was to insert the lens and iteratively adjust its location and orientation so that the red beam was focused on the chip, and further that the reflections from the front and back surfaces of the lens overlapped and were centered on the input beam. An interference pattern was discernible on the near iris when the orientation was proper. The red beam was then brought to a near focus on the laser facet; the additional focus distance changes were made with the infrared beam. The third step takes place when the chamber is evacuated and only translation of the focusing lens is possible. A red beam through the irises (away from the chamber) is used to locate a detector at a fixed position on the optic axis about 60 cm past the second external iris. With the TDL operational, the focusing lens was manipulated for maximum signal on the detector, insuring that the infrared beam and the red beam were as collinear as possible. A partly transmitting reflector (nominal reflectance = 80%) is placed outside the chamber (about 10 cm from the chamber window)

at normal incidence to the TDL beam as determined by the retroreflected red beam which again is toward the chamber. A short focal length lens is then inserted and adjusted in front of the detector to return the attenuated beam to a usable signal level on the oscilloscope.

The second phase of the feedback adjustment begins with a triangular modulation of the TDL current and a display of the intensity versus current on a oscilloscope. The current is adjusted so that the sweep is centered about threshold current. The effect of the feedback on the lasers is a decrease in the threshold current. With the two orthogonal controls on the translator stage fixed, the focus control is used to move the lens along the optical axis until the threshold point in the P-I curve abruptly jumps toward lower current. For the lead-salt laser the range of significant feedback is a displacement of the lens of about 3×10^{-4} of the nominal 25.4 mm focal length. Once the initial effect of feedback is found, the beam splitter (or grating) orientation and the two lens controls orthogonal to the focus control can be used to maximize the feedback.

3.3 The Diode Lasers

The TDLs used in this work were $Pb_{1-x}Eu_xSe_yTe_{1-y}/PbTe$ double heterostructures (DH) in the buried heterostructure (BH) configuration. The Eu content is about 3%. The BH configuration is of advantage for extended-cavity experiments since this design should exhibit very little astigmatism. All lasers were designed to operate in the temperature range above 80 K and in the wavelength region near 3.4 μm ($\approx$ 3000 cm^{-1}). The laser chips were mounted in a standard submount which allows access to only one of the two output facets.

Nine lasers were obtained for this investigation. Four of these nine lasers were considered for coating. They showed relatively high output power and worked in a single longitudinal mode for certain current/temperature conditions.

3.4 Characterization of the TDL Emission Properties

The emission properties of the diode lasers were evaluated before and after a coating run as well as in different extended-cavity configurations. Three different optical paths were used (switchable by means of kinematic mirror mounts) for three different purposes. To

analyze the spectral mode behavior, the TDL beam was fed through a monochromator (resolution = 0.1 cm^{-1}). This permitted recording and calibration of the emission spectrum under different operation conditions (temperature and current). To measure the spectral linewidth of a TDL mode, the diode laser output was directed to a fast HgCdTe photodetector and heterodyned against the output of a CO gas laser which served as the local oscillator. This CO laser operates in the ($\Delta\ v = 2$) mode, and provides a large number of laser lines in the wavelength region of interest (typical frequency gap = 4 cm^{-1}). The spectral width of the CO laser was previously determined to be about 100 kHz. To characterize the threshold behavior of the TDL the beam was fed directly into a liquid-nitrogen-cooled InSb photodiode and the laser output power was recorded versus the laser current (P-I plot). These plots are a useful monitor of the change in threshold and slope efficiency after coating (Sec. 4.1).

4 Results and Discussion

4.1 Coating Experiments

As pointed out in Sec. 2.2, an AR coating of the TDL output facet is needed to achieve good extended-cavity performance. Although dielectric AR coatings are commonly applied to NIR diode lasers, no successful coating attempt for Pb-salt lasers has been published to date. During preparation of the manuscript a group at the Fraunhofer Institute (IPM) in Freiburg, Germany, indicated that they are working on similar coatings in the 10 μm region. Coating technology in the MIR wavelength region is more difficult than in the visible or NIR because of coating material limitations. A further difficulty is that the coating must withstand the temperature cycling of the lasers. Table 2 summarizes the materials employed for coating.

For the first coating attempt, we chose to apply a single $\lambda/4$ layer (for $\lambda = 3.4\ \mu$m) of zinc selenide (ZnSe, $n = 2.4$ at 3 μm), a common infrared material, to laser A. After coating, the residual reflectance of the coated facet was determined by means of a reflectometer to be below 1%. The reflectometer operates in the visible spectral region, thus the minima of reflectance at $\lambda/5$ and $\lambda/7$ were measured. Since these coating materials show absorption in

Table 2: Coating materials.

Laser	1. Layer	2. Layer	3. Layer	4. Layer
A	ZnSe ($1/4 \times 3.4$ μm)			
B	Sb_2S_3 ($1/4 \times 3.4$ μm)			
C	Sb_2S_3 (630 nm)	SiO (425 nm)*		
D	Si (750 nm)	SiO (207 nm)	Na_3AlF_6 (315 nm)	SiO (207 nm)

Numbers in parentheses are optical thicknesses n·d.

*A better value of n·d for SiO is 390 nm.

the visible, the reflectometer measurements can give only a rough estimate of the infrared reflectance.

Though the ZnSe coating seemed to lower the facet reflectance considerably, the laser threshold measurement yielded no significant increase of the threshold after coating. Obviously, the ZnSe coating did not adhere well to the laser facet. This was confirmed after warm-up by examining the laser facet under a microscope. The reason for this is probably the considerable mismatch of thermal expansion. The thermal coefficient of linear expansion for ZnSe is approx. 2 to 7×10^{-6}/ K between 77 and 300 K, whereas the expansion coefficient for PbTe is approximately 2×10^{-5}/ K in the same temperature region.

Another promising IR coating material is antimony sulfide (Sb_2S_3, $n = 2.8$ at 3 μm). Laser B was coated with a $\lambda/4$ layer (for $\lambda = 3.4$ μm), the reflectometer again indicated a residual reflectance below 1%. In this case, recording of the P-I plot revealed a significant change in both threshold and slope efficiency. Fig. 3 shows the P-I plots at $T = 87$ K before and after coating. The threshold was increased by 12 to 15% after the coating. We temperature-cycled the coated diode several times and observed only minor changes in the threshold and slope behavior which arise from slight changes in the mode characteristics after each cycle. Thus, we concluded that the Sb_2S_3 coating adheres well to the laser facet.

In order to obtain the actual residual reflectance from the threshold increase by means of eqs (7) and (8), one needs to know the internal gain parameter γ, which is not available.

Another way to determine the residual reflectance is to analyze the change of the slope efficiency. It is difficult to obtain an absolute number for the slope $\Delta P/\Delta I$ due to large

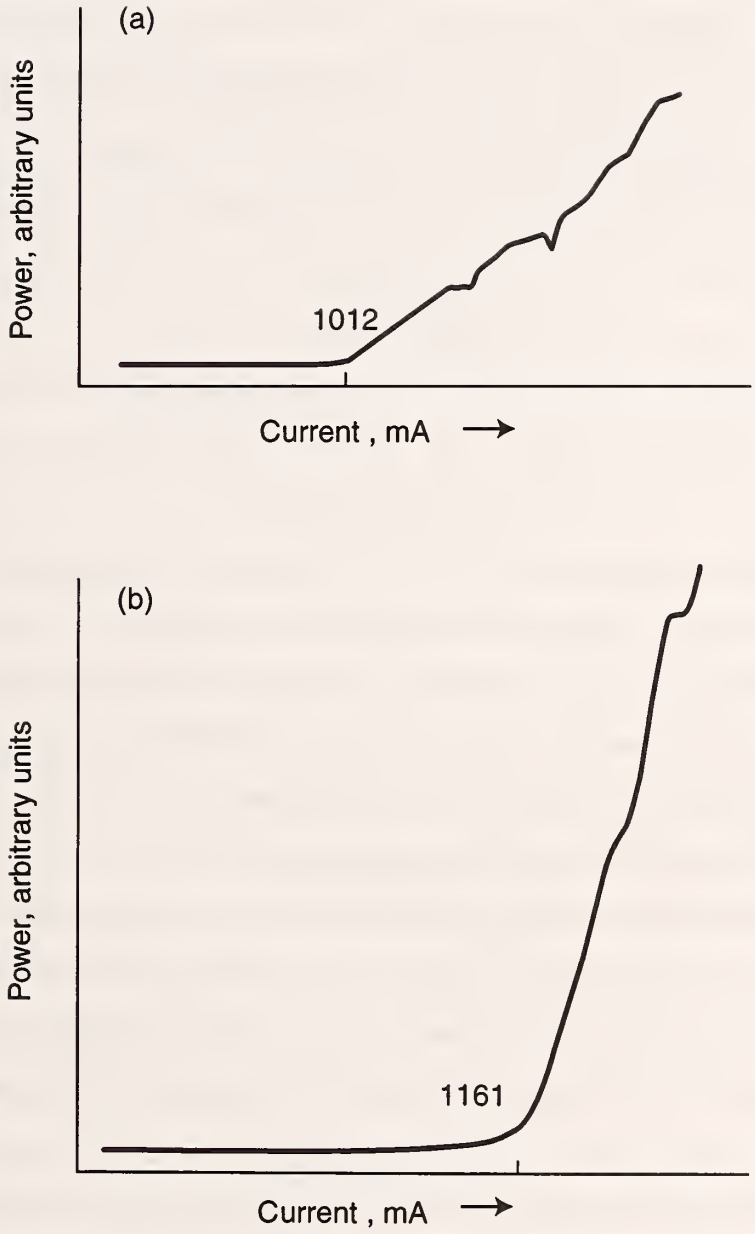

Figure 3: P-I plots of laser B at $T = 87$ K, (a) before coating, and (b) after coating with a single layer of Sb_2S_3.

uncertainties in the alignment, transmittance of optical elements, photodiode calibration, etc. However, a rough estimate of the residual reflectance can be obtained from the relative change of the slope efficiency before and after coating as follows.

According to eqs (15) and (16) the change of the slope efficiency is directly related to the change in the mirror reflectances. If the power reflectance of the uncoated facet is 45%, the observed slope increase by a factor of 4 to 5 translates into a decrease of the power reflectance to something on the order of 1%. For this calculation α_{int} was estimated to be about 10^5 m^{-1}. This result now allows us to estimate the internal gain parameter γ. From eqs (7) and (8) we obtain

$$\gamma = \frac{\ln(r_1/r_2^*)}{L_{\text{int}}\,(I_{\text{th}}^{\text{AR}} - I_{\text{th}})}\,, \tag{17}$$

yielding $\gamma = 0.03$ $\text{mA}^{-1}\cdot\text{mm}^{-1}$. This value is an order of magnitude lower than the corresponding value for a typical GaAs diode laser (Table 1). Unfortunately, this laser diode stopped working two weeks after coating for unknown reasons.

Since the Sb_2S_3 coating adhered very well to the laser, we were encouraged to try a double-layer coating, based on Sb_2S_3. Multilayer dielectric coatings permit a lowering of residual reflectance and are also used to broaden the low-reflectance bandwidth. Laser C was coated with a layer of Sb_2S_3 and an additional layer of SiO (Table 2). Due to difficulties with the coating apparatus the coating was nominally best for $\lambda = 3.6$ μm instead for $\lambda = 3.4$ μm. The calculated reflectance has a minimum of 10^{-4} at $\lambda = 3.6$ μm assuming a refractive index of n = 6 for the substrate. The threshold increase observed with this coating was 8 to 10%. The characterization of this laser was complicated by the fact that the mode pattern changed significantly after each temperature cycle. This also affects the threshold. It is certainly worthwhile to try this type of double-layer coating once more with another diode laser.

For the final coating attempt, laser D was coated with the four layers listed in table 2. The calculated reflectance was below 0.1% between $\lambda = 3.25$ μm and 3.69 μm, and the minimum reflectance was about 10^{-4} at $\lambda = 3.5$ μm. After coating the laser threshold was increased by 10% which was quite reproducible during several temperature cycles. Our longer view of these 4 coatings is (see p. 19) that the Sb_2S_3 and SiO combination is the best

coating choice for these high index lasers. Optical tests indicated that this coating gives the lowest reflectivity, and the coating was still functional one year later.

We note that the high internal loss in these lead-salt lasers reduces the amount of threshold change with facet reflectance when compared with results for AlGaAs lasers.

4.2 Extended-Cavity Experiments

After the first successful AR coating (laser B) we started to explore the performance in the extended-cavity mode. In the early stage of the investigations we tried an off-axis parabola (OAP) for collimation of the diverging diode laser beam. However, with this arrangement we obtained only a very low optical feedback level. Some narrowing of the laser linewidth was observed in a heterodyne experiment, but we did not observe any effect on the laser threshold; obviously the round-trip loss in the external cavity was too large. The OAP provides perfect collimation of a point-like radiation source which is located at the focal point of the parabola. However, an OAP shows greater aberrations for a small alignment error than does a lens. That means that the alignment of the OAP is very critical. In our case it turned out to be extremely difficult and time-consuming to achieve good OAP alignment. Another difficulty in using an OAP for diode laser collimation arises from the fact that the diode is NOT a point-like radiation source. The diode laser beam emerges from an area of about 0.5×2.6 μm and exhibits astigmatism.

After a careful examination of the OAP alignment with the TDL as well as with a visible diode laser beam, we concluded that the OAP is not the best choice for our purpose. Thus, we decided to modify the cryostat optics to use a lens to collimate the TDL beam (Fig. 2). A lens is much more forgiving regarding small deviations of the radiation source from the focal point. However there is a well-known imaging error, namely spherical aberration. Spherical aberration is most important for small f numbers and for low-index materials. For the MIR spectral region, meniscus-shaped lenses exhibit lower spherical aberration than plano-convex lenses [10]. Figure 4 shows the focal spot size versus the diameter of a (collimated) input beam for a ZnSe plano-convex lens with a focal length of 25.4 mm. The left part of the graph is dominated by diffraction whereas the rise of the curve in the right part is caused by

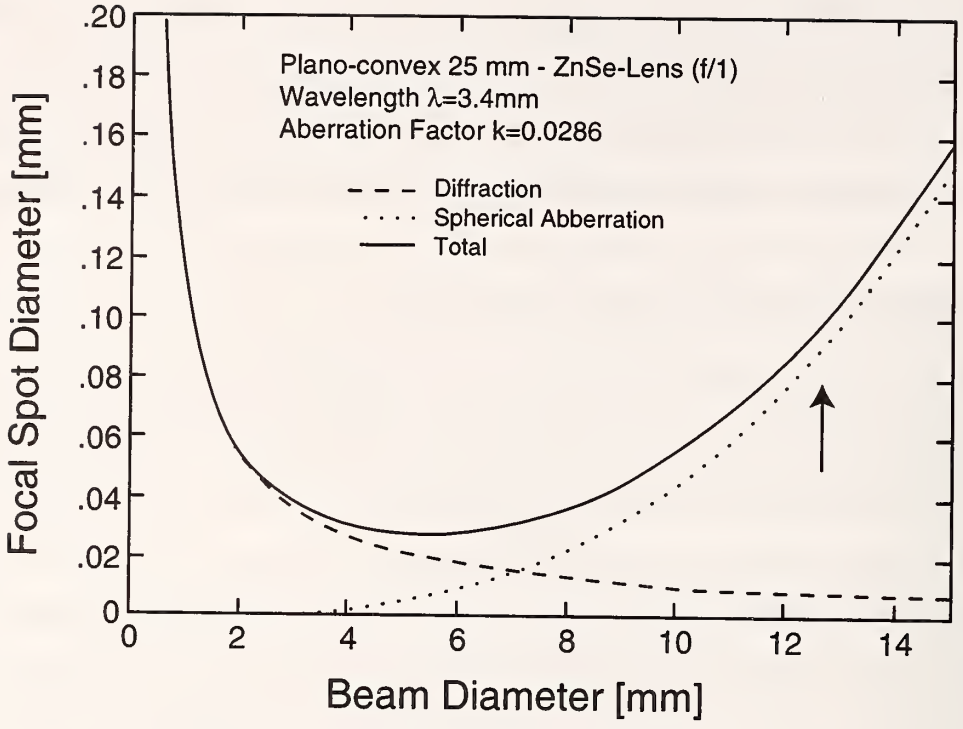

Figure 4: Calculated focal spot diameter versus input beam diameter for plano-convex zinc selenide lens, 25.4 mm focal length. Curves are calculated after [10]. The arrow indicates the region of interest for TDL collimation.

spherical aberration. For the collimation of lead-salt diode radiation $f/2$ optics is required. This value – marked with an arrow – is clearly in the region where spherical aberration is most important. The best choice for low imaging errors is thus a lens which is compensated for spherical aberration and coma. Another possibility is a lens doublet or triplet, which consists of a matched lens system optimized for low aberration. Both ways have been shown to be successful with NIR diode lasers.

Since an IR aspheric lens was not available initially, we examined the imaging properties of several available lenses and lens combinations. For this purpose the lens under investigation was used to focus the CO laser beam, and the focus diameter was measured with a razor blade on a translation stage. The tightest focus was achieved – as expected – with a germanium meniscus lens. However, since germanium is not transparent in the visible, there is no way to prealign the lens by means of a red HeNe laser. Next, we tried a lens made of ZnSe. This was a $f/1$ plano-convex lens, AR coated for $\lambda = 3$ μm, with a focal length of

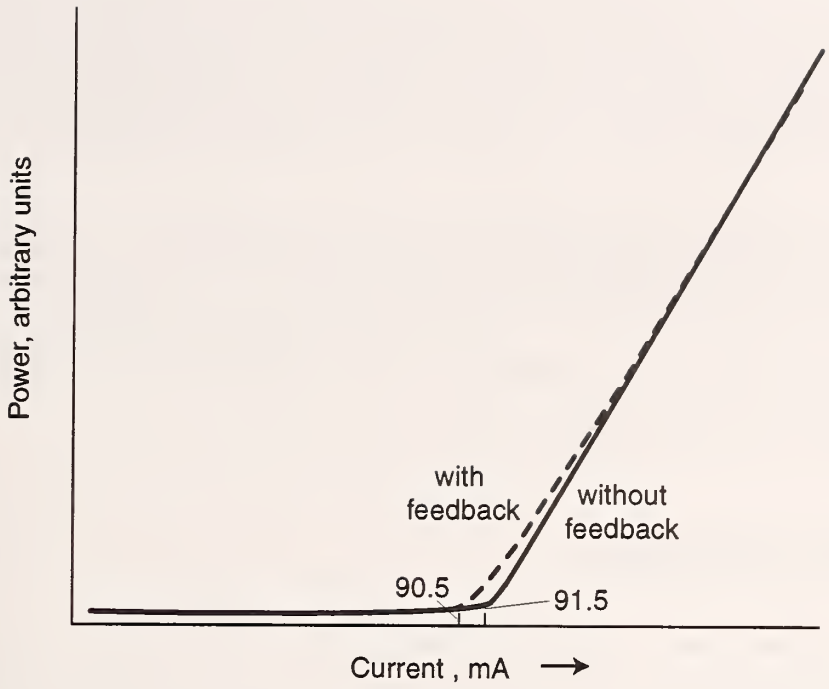

Figure 5: P-I plots of laser D after coating, with and without feedback from an external 80% reflector. Collimation is achieved with a plano-convex ZnSe lens.

25.4 mm. The transmittance at $\lambda = 3.4$ μm was measured to be $\geq 93\%$. A nearly collimated CO laser beam of 5 mm diameter is focussed down to a spot diameter of 35 μm by this lens.

For the feedback experiments with lens collimation, we used laser D which was broadband AR-coated with four layers (Table 2). As described in section 3.2, we started with an 80% reflector as external feedback mirror. The threshold of the laser was increased by 10% as a result of the AR coating and we hoped to bring the threshold almost back to its original value by means of the extended cavity. However, the most we could decrease the threshold by was 1% (from 91.5 mA to 90.5 mA) with external feedback. The slope efficiency changed correspondingly. This is depicted in Fig. 5. The coupling loss due to aberration errors of the collimating lens is difficult to measure. Therefore, the effective external reflectance could not be determined. However, the small change of the threshold current clearly shows that the external reflectance is far too low for good extended-cavity performance.

Eight months after a temporary halt of the work an aspheric lens became available. After integration of the new lens we observed a much stronger feedback effect on the threshold

current. For this experiment we chose laser C which was AR-coated with a layer of Sb_2S_3 and an additional layer of SiO (Table 2). The threshold current of the laser was increased by 8 to 10% due to the AR coating. With optical feedback from the external 80% reflector we achieved a threshold decrease from 124 to 121 mA; this is about 2.5% back toward the precoating value.

In order to achieve a better understanding of these experimental results a better knowledge of the lead-salt diode properties is needed. Exact knowledge of material parameters, such as internal optical loss and gain, is essential in order to exactly determine the residual facet reflectance, effective external reflectance, etc.

5 Concluding Remarks

In conclusion, we have developed an extended-cavity TDL vacuum chamber with liquid nitrogen cooling and servo control of the temperature of the TDL mounting platform. The chamber contains the essential feedback optics and we have established a procedure for aligning the optics and optimizing the feedback. We have had success with applying a combination of Sb_2S_3 and SiO coating to these $n = 6$ lead-salt lasers (residual reflectance on the order of 1%). However, grating control seems just beyond our control at present. The same set-up and procedure was recently used to investigate the operation of novel InAsSb diode lasers for 3 μm in an ECGT configuration [11]. In this case we were able to tune an uncoated laser over 50 cm^{-1} with the grating (but with a very limited sample of devices have yet no success with our coated lasers). One possible source of difficulty with grating control of the lead-salt lasers is their spatial mode structure which is complex. A suitable IR camera for analysis of the spatial beam profile would greatly facilitate future investigations of external-cavity lead-salt lasers. Another possible source of difficulty is that the internal photon losses require a higher level of optical feedback than our present scheme affords. One means to increase the feedback by a factor of nearly 2 would be to return to the original two-sided output design we initially studied in Bonn, and return all of the power from the grating on the feedback side.

Acknowledgements

We are appreciative of the cooperation by Laser Photonics, Inc., Analytics Division [12] who supplied the lasers, furnished us a surplus closed-cycle cooler TDL mounting platform, and provided useful information about their new high-temperature TDLs. We also thank R. Fox and S. Waltman of our group for useful information and contributions. One of us (MM) acknowledges support from the Deutsche Forschungsgemeinschaft (DFG), and is grateful for the warm hospitality during his stay at NIST.

References

[1] Mürtz, M.; Schaefer, M.; Schneider, M.; Wells, J.S.; Urban, W.; Schiessl, U.; Tacke, M. Stabilization of 3.3 and 5.1 μm lead-salt diode lasers by optical feedback. Opt. Commun. 94(6): 551–556; 1992.

[2] Mürtz, M.; Schaefer, M.; George, T.; Wells, J.S.; Urban, W. Optically stabilized tunable diode-laser system for saturation spectroscopy. Appl. Phys. B 60: 31–37; 1995.

[3] Dahmani, B.; Hollberg, L.; Drullinger, R. Frequency stabilization of semiconductor lasers by resonant optical feedback. Opt. Lett. 12(11): 876–878; 1987.

[4] Petermann, K. Laser diode modulation and noise. Dordrecht: Kluwer Academic Publ.; 1988. 315 p.

[5] Ohtsu, M. Highly coherent semiconductor lasers. Boston: Artech House; 1992. 340 p.

[6] Zorabedian, P. Tunable external-cavity semiconductor lasers, chapter in Tunable lasers handbook. Duarte, F.J., ed. San Diego: Academic Press; 1995. 349–442.

[7] Suematsu, Y.; Adams, A.R., eds. Handbook of semiconductors and photonic integrated circuits. London: Chapman & Hall; 1994. 546 p.

[8] Emtage, P.R. Auger recombination and junction resistance in lead-tin telluride. J. Appl. Phys. 47(6): 2565–2568; 1976.

[9] Olsson, A.; Tang, C.L. Coherent optical interference effects in external-cavity semiconductor lasers. IEEE J. Quantum Electron. QE-17(8): 1320–1323; 1981.

[10] II-VI, Inc.* Optics Catalog; 1995.

[11] Mürtz, M., Wells, J.S., Hollberg, L., Zibrova, T., and Mackie, N. Extended-cavity grating-tuned operation of a mid-infrared InAsSb diode laser near 3 μm. to be published in Appl. Phys. B (1997).

[12] Laser Photonics, Inc.*, Analytics Division, 10 Upton Drive, Wilmington MA 01887.

*Certain commercial materials or equipment are identified in this paper in order to specify the experimental procedure. Such identification does not imply recommendation or endorsement by the National Institute of Standards and Technology.

*U.S. GOVERNMENT PRINTING OFFICE 1997-0-573-018/40066

NIST Technical Publications

Periodical

Journal of Research of the National Institute of Standards and Technology—Reports NIST research and development in those disciplines of the physical and engineering sciences in which the Institute is active. These include physics, chemistry, engineering, mathematics, and computer sciences. Papers cover a broad range of subjects, with major emphasis on measurement methodology and the basic technology underlying standardization. Also included from time to time are survey articles on topics closely related to the Institute's technical and scientific programs. Issued six times a year.

Nonperiodicals

Monographs—Major contributions to the technical literature on various subjects related to the Institute's scientific and technical activities.

Handbooks—Recommended codes of engineering and industrial practice (including safety codes) developed in cooperation with interested industries, professional organizations, and regulatory bodies.

Special Publications—Include proceedings of conferences sponsored by NIST, NIST annual reports, and other special publications appropriate to this grouping such as wall charts, pocket cards, and bibliographies.

Applied Mathematics Series—Mathematical tables, manuals, and studies of special interest to physicists, engineers, chemists, biologists, mathematicians, computer programmers, and others engaged in scientific and technical work.

National Standard Reference Data Series—Provides quantitative data on the physical and chemical properties of materials, compiled from the world's literature and critically evaluated. Developed under a worldwide program coordinated by NIST under the authority of the National Standard Data Act (Public Law 90-396). NOTE: The Journal of Physical and Chemical Reference Data (JPCRD) is published bimonthly for NIST by the American Chemical Society (ACS) and the American Institute of Physics (AIP). Subscriptions, reprints, and supplements are available from ACS, 1155 Sixteenth St., NW, Washington, DC 20056.

Building Science Series—Disseminates technical information developed at the Institute on building materials, components, systems, and whole structures. The series presents research results, test methods, and performance criteria related to the structural and environmental functions and the durability and safety characteristics of building elements and systems.

Technical Notes—Studies or reports which are complete in themselves but restrictive in their treatment of a subject. Analogous to monographs but not so comprehensive in scope or definitive in treatment of the subject area. Often serve as a vehicle for final reports of work performed at NIST under the sponsorship of other government agencies.

Voluntary Product Standards—Developed under procedures published by the Department of Commerce in Part 10, Title 15, of the Code of Federal Regulations. The standards establish nationally recognized requirements for products, and provide all concerned interests with a basis for common understanding of the characteristics of the products. NIST administers this program in support of the efforts of private-sector standardizing organizations.

Consumer Information Series—Practical information, based on NIST research and experience, covering areas of interest to the consumer. Easily understandable language and illustrations provide useful background knowledge for shopping in today's technological marketplace.
Order the **above** *NIST publications from: Superintendent of Documents, Government Printing Office, Washington, DC 20402.*
Order the **following** *NIST publications—FIPS and NISTIRs—from the National Technical Information Service, Springfield, VA 22161.*

Federal Information Processing Standards Publications (FIPS PUB)—Publications in this series collectively constitute the Federal Information Processing Standards Register. The Register serves as the official source of information in the Federal Government regarding standards issued by NIST pursuant to the Federal Property and Administrative Services Act of 1949 as amended, Public Law 89-306 (79 Stat. 1127), and as implemented by Executive Order 11717 (38 FR 12315, dated May 11, 1973) and Part 6 of Title 15 CFR (Code of Federal Regulations).

NIST Interagency Reports (NISTIR)—A special series of interim or final reports on work performed by NIST for outside sponsors (both government and non-government). In general, initial distribution is handled by the sponsor; public distribution is by the National Technical Information Service, Springfield, VA 22161, in paper copy or microfiche form.

U.S. Department of Commerce
National Institute of Standards and Technology
325 Broadway
Boulder, Colorado 80303-3328

Official Business
Penalty for Private Use, $300